Increase of global monsoon area and precipitation under global warming: A robust signal?

Pang-chi Hsu,[1] Tim Li,[1] Jing-Jia Luo,[2] Hiroyuki Murakami,[3,4] Akio Kitoh,[4] and Ming Zhao[5]

Received 20 January 2012; revised 18 February 2012; accepted 20 February 2012; published 16 March 2012.

[1] Monsoons, the most energetic tropical climate system, exert a great social and economic impact upon billions of people around the world. The global monsoon precipitation had an increasing trend over the past three decades. Whether or not this increasing trend will continue in the 21st century is investigated, based on simulations of three high-resolution atmospheric general circulation models that were forced by different future sea surface temperature (SST) warming patterns. The results show that the global monsoon area, precipitation and intensity all increase consistently among the model projections. This indicates that the strengthened global monsoon is a robust signal across the models and SST patterns explored here. The increase of the global monsoon precipitation is attributed to the increases of moisture convergence and surface evaporation. The former is caused by the increase of atmospheric water vapor and the latter is due to the increase of SST. The effect of the moisture and evaporation increase is offset to a certain extent by the weakening of the monsoon circulation. **Citation:** Hsu, P., T. Li, J.-J. Luo, H. Murakami, A. Kitoh, and M. Zhao (2012), Increase of global monsoon area and precipitation under global warming: A robust signal?, *Geophys. Res. Lett.*, *39*, L06701, doi:10.1029/2012GL051037.

1. Introduction

[2] The monsoon circulation is generally characterized by a seasonal reverse in lower tropospheric winds in response to large-scale continent-ocean thermal contrast [*Webster*, 1987]. The rainfall over the monsoon regions exhibits a great seasonal contrast, and the variability of the monsoon rain exerts not only a socioeconomic impact upon two-third of the world's population living in the area but also an influence throughout the global ecosystem. While individual monsoon systems have their own evolution characteristics, the concept of the global monsoon was introduced, to describe the overall strength of the monsoon systems around the globe [*Trenberth et al.*, 2000; *Wang and Ding*, 2006]. A recent observational study shows that the global monsoon area (GMA) and the global monsoon total precipitation (GMP) have increased during 1979–2008 [*Hsu et al.*, 2011; *Wang et al.*, 2012]. Whether this increasing trend will continue in a future potentially warmer climate throughout the 21st century is an important issue that needs to be addressed.

[3] A key issue to future climate projection is whether a signal projected is robust across different model physics and future warming patterns. While the increase of air temperature is projected consistently among models, projection in precipitation tends to be model-dependent [*Neelin et al.*, 2006; *Xie et al.*, 2010]. In addition, the future rainfall projection may be resolution-dependent. Most models participated in the Coupled Model Intercomparison Project Phase 3 and Phase 5 (CMIP3 and CMIP5) had a horizontal resolution of roughly 200 km. It has been pointed out that higher resolution general circulation models (GCMs) generally reproduced a better spatial pattern of the global monsoon rainfall compared to lower-resolution models [*Kim et al.*, 2008]. To increase confidence in the future projection, in this study we compared simulations from three high-resolution GCMs forced by different future SST warming patterns. The goal of this study is to seek consistent and robust signals across different model physics and different SST patterns.

2. Model Experiment Design and Methodology

[4] The three high-resolution atmospheric GCMs (AGCMs) employed here are 1) the Max Planck Institute (MPI) ECHAM5 [*Roeckner et al.*, 2003] at T319 (∼40 km) resolution, the Japan Meteorological Research Institute MRI-JMA [*Mizuta et al.*, 2006] at T959 (∼20 km) resolution, and the US Geophysical Fluid Dynamics Laboratory (GFDL) High-Resolution Atmospheric Model (HiRAM) [*Zhao et al.*, 2009] at C180 (∼50 km) resolution. It is worth mentioning that the three high-resolution models have different treatments in key physics parameterizations, including the representations of moist convection, large-scale stratiform clouds, the planetary boundary layer turbulence as well as cloud radiation. For example, for the moist convection parameterization, ECHAM5 uses a *Tiedtke* [1989] scheme modified by *Nordeng* [1994], HiRAM uses a modified *Bretherton et al.* [2004] scheme, and MRI AGCM uses a prognostic Arakawa and Schubert convection scheme [*Randall and Pan*, 1993]. Thus it is our intention to use these models to examine the sensitivity of future projection to different model physics and to identify robust features among these models.

[5] A 'time-slice' method [*Bengtsson et al.*, 1996] was applied, in which the AGCMs are forced by present-day and future warming SST fields. The details of each model experiment are described in Table 1. For the present-day simulations, either observed SST or simulated historical SST field of 20C3M [*Meehl et al.*, 2007] were used. A diagnosis of

[1]International Pacific Research Center, University of Hawaii at Manoa, Honolulu, Hawaii, USA.
[2]Centre for Australian Weather and Climate Research, Melbourne, Victoria, Australia.
[3]Japan Agency for Marine-Earth Science and Technology, Yokohama, Japan.
[4]Climate Research Department, Meteorological Research Institute, Tsukuba, Japan.
[5]Geophysical Fluid Dynamics Laboratory, NOAA, Princeton, New Jersey, USA.

0094-8276/12/2012GL051037

Table 1. Model Experiment Designs

Model	Present-Day Simulations		Global Warming Experiments	
	Acronym	SST Forcing	Acronym	SST Forcing
MPI ECHAM5 T106 (~**1.125º**)	**T106_pd**	AMIP-type run with observed SST in 1978–1999	**T106_mw**	AMIP SST in 1978–1999 plus a globally uniform SST warming (2.24°C) which is the global average of ECHAM5/MPI-OM simulated SST anomaly between A1B (2080–2100) and 20C3M (1980–2000)
			T106_sw	AMIP SST in 1978–1999 plus a spatially-varying SST warming pattern derived from ECHAM5/MPI-OM simulated SST anomaly between A1B (2080–2100) and 20C3M (1980–2000)
MPI ECHAM5 T319 (~**40 km**)	**T319_pd**	ECHAM5/MPI-OM simulated SST in 20C3M (1980–2000)	**T319_sw**	ECHAM5/MPI-OM simulated SST in A1B (2080–2100)
Japan MRI-JMA T959 (~**20 km**)	**MRI_pd**	Historical 1979–2003 HadISST	**MRI_sw.e**	Sum of present-day (1979–2003) SST annual and interannual variations and a linear trend of future SST change derived from 18 CGCMs in CMIP3 in A1B
US GFDL HiRAM C180 (~**50 km**)	**GFDL_pd**	Historical 1982–2005 HadISST	**GFDL_sw.e**	Future SST warming pattern [by differencing 2080–2100 (A1B) SST from the 2001–2020 SST] derived from 18 CMIP3 CGCMs was added to 1982–2005 HadISST climatology

the present-day simulations shows that the models are capable of reproducing the observed annual mean precipitation pattern and the global monsoon domain, which adds the confidence in projecting future changes. For future simulations, SST in ECHAM5 was derived from a lower-resolution (T63) coupled ECHAM5/MPI ocean model (MPI-OM) [*Jungclaus et al.*, 2006] simulation in A1B scenario for period 2080–2010, whereas SST in the MRI and GFDL models was derived from the ensemble average of 18 IPCC AR4 models for the same period. To examine the sensitivity of future projection to model resolution, additional two experiments with ECHAM5 T106 (~1.125º) were conducted. In the first sensitivity experiment, the future SST pattern is similar to that of T319. In the second sensitivity experiment a uniform 2.24°C warming SST pattern was applied.

[6] We followed the definition of the GMA used by *Liu et al.* [2009]. The GMA is defined by the regions where (1) the annual range of precipitation exceeds 2 mm day^{-1} and (2) the local summer precipitation exceeds 55% of annual rainfall. Here the 'annual range' is defined as the difference of rainfall between local summer and winter [May-September for northern summer (southern winter) and November-March for northern winter (southern summer)]. Considering possible changes in the annual rainfall range under global warming, we conducted a sensitivity test by using different criteria of summer-to-annual rainfall ratios (e.g., 45%, 50%, 55%, 60%, 65%) to derive the GMA. The change rates of GMA associated with warming climate are not sensitive to the ratios. The GMP is defined as the sum of total summer rainfall in the monsoon area. Because the actual area of each grid changes with latitude, an area-weighting metric was used for calculations of the GMA and GMP. A global monsoon intensity (GMI) index was defined to measure the global monsoon precipitation amount per unit area [*Hsu et al.*, 2011].

3. Results

[7] Figure 1 (top) displays the composite present-day GMA (red contour) and the composite future GMA change (shaded area). Here the composite is based on the five simulations described in Table 1. The high-resolution AGCMs capture well the major monsoon areas in the present-day simulations, including the Asian, Australian, North American, South American, West African and South African monsoons, although the models tend to extend the oceanic monsoon regions compared to the observation [see *Liu et al.*, 2009, Figure 2]. The global warming expands the GMA (represented by blue shaded areas) over most of the monsoon regions, except for small areas in the subtropics near 20º–30º north and south (orange shaded areas). The marked expansions occur in the oceanic monsoon regions, which accounts for 80%–90% contribution to the GMA change. It is noted that the increased GMA is attributed to not only an increased annual range of precipitation under global warming [*Chou and Lan*, 2012] but also a stronger summer-to-annual rainfall ratio in future climate. The consistent increase of the GMA appears in all five simulations. The change rate in the GMA from the present-day to the future simulations is 7.8%, 4.6%, 8.7%, 7.2% and 6.6% based on the T106_mw, T106_sw, T319_se, MRI_sw.e and GFDL_sw.e experiments, respectively. Figure 1 (middle top) shows that the averaged increase rates of the GMA are about 7%–9%, regardless the calculations being based on individual model simulations or based on the composite. The consistent increase of the GMA among all simulations reveals that it is a robust signal across different model physics and different future SST warming patterns.

[8] Besides the GMA expansion, another consistent feature among the five simulations is an increase of the global monsoon total precipitation. The increase rates of the GMP range from 7% in the GFDL to 20% in the T106_mw experiments (9.9%, 10.4% and 15.2% in the MRI_sw.e, T106_sw and T319_sw simulations respectively). The averaged increase rates based on the five individual simulations and based on the rainfall composite are 13% and 16%, respectively. Both the monsoon precipitation over land and oceanic regions are enhanced. About 40% (60%) contribution of the GMP increase is from land (oceanic)

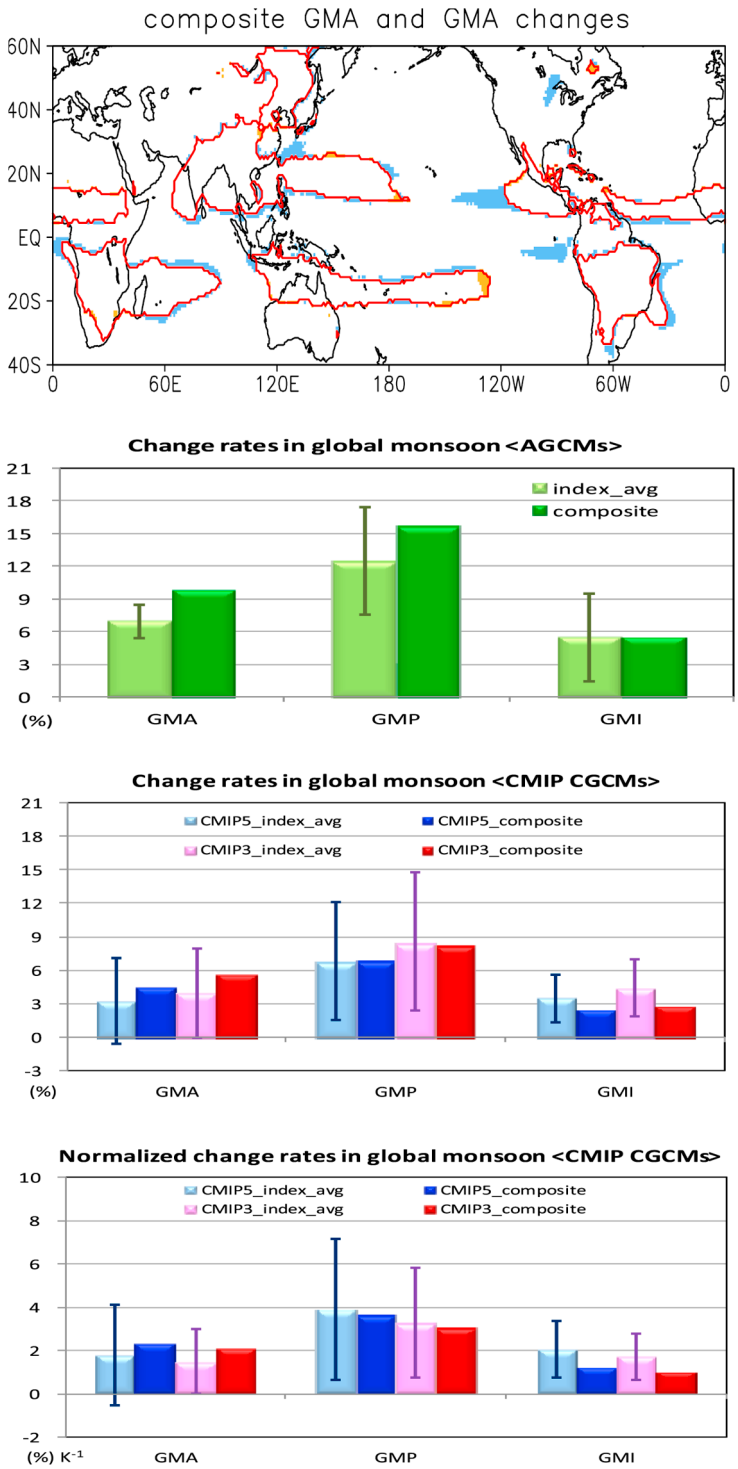

Figure 1. Changes in GMA, GMP and GMI under global warming. (top) Difference of the GMA (shaded) between the global warming and present-day simulations derived from the composite of simulated precipitation fields. Red contours denote the composite GMA in the present-day simulations. Blue (orange) shading indicates the increase (decrease) of the GMA. (middle top) Changes rates (%) in the GMA, GMP and GMI between the global warming and present-day simulations. Light color bars are the averages of the monsoon indices from five AGCM simulations with whiskers denoting one standard deviation. Dark color bars show the calculations based on the composite precipitation fields. (middle bottom) Same as Figure 1 (middle top) except that the change rates are calculated based on the differences of 11 CMIP5 CGCM simulations between RCP4.5 (2075–2099) and Historical (1979–2003) scenarios (red bars), and the differences of 24 CMIP3 CGCM simulations between 20C3M (2075–2099) and A1B (1979–2003) scenarios (blue bars). (bottom) Same as Figure 1 (middle bottom) but global monsoon change rates are normalized by globally averaged surface air temperature changes (unit: % K^{-1}).

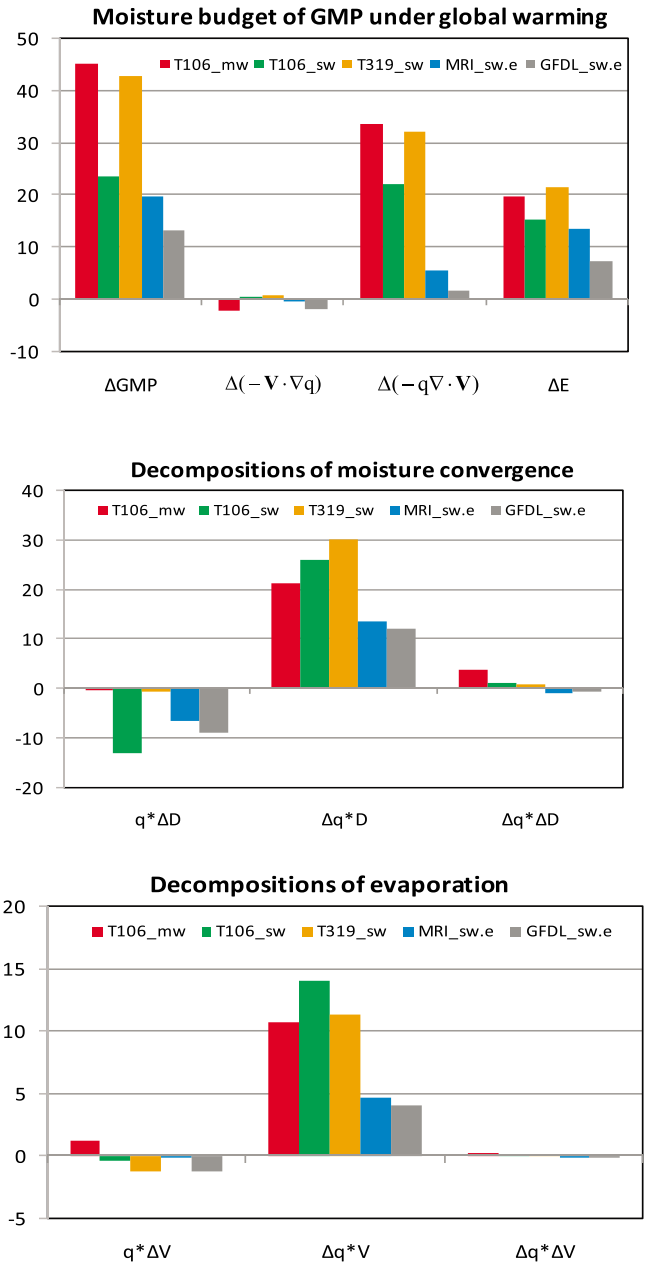

Figure 2. Moisture processes responsible for the GMP increase. (top) Change of the future GMP from five simulations and relative contributions of moisture advection, moisture convergence and surface evaporation within GMA. Unit is 10^{14}W. (middle) Contribution of the moisture convergence by the circulation change, the moisture change and the nonlinear product of the two changes. (bottom) Contribution of the surface evaporation by the circulation change, the moisture change and the nonlinear product of the two changes.

monsoon region. The increasing rates of GMP are larger than the increasing rates of GMA, implying that the global monsoon intensity, which is defined as the monsoon precipitation amount per unit area, tends to strengthen in the future warmer climate. Our calculation shows that the GMI has an averaged increase rate of about 5% (Figure 1, middle top). It is worthy to mention that the intensification of GMI is mainly contributed from the land monsoon region (60–70%) rather than from the oceanic monsoon region (30–40%). The enhanced GMI over land would exert great impacts on the large population living in the monsoon regions.

[9] The results above were derived based on the time slice method. To examine whether the results depend on the integration method, we applied the same analysis methodology to 11 (24) CMIP5 (CMIP3) atmosphere-ocean coupled GCM (CGCM) outputs. The projected future GMA, GMP and GMI changes were plotted in Figure 1 (middle bottom). Since the CMIP experiments tend to show great variations in the magnitude of global warming by the end of 21st century, the global monsoon changes normalized by the surface warming are also shown in Figure 1 (bottom). It shows that the averaged changes among the CMIP5/CMIP3 models agree well with the current high-resolution simulations. Most of individual CMIP5/CMIP3 models projected the increases in GMA, GMP and GMI under future warming scenarios. The increasing rate of GMP (GMA and GMI) is around 3–4% (1–2%) when the global surface air temperature increases 1 K. This suggests that the enhanced GMA, GMP and GMI are not model-dependent phenomena, nor do they depend on a specific SST warming pattern.

[10] To address what contributes to the increase of the global monsoon precipitation, we examine a column-integrated moisture budget within the GMA in the present-day and future warming simulations, respectively. The column-integrated moisture tendency equation is

$$\frac{\partial w}{\partial t} + < \nabla \cdot (q\mathbf{V}) >= E - P \qquad (1)$$

where w is the precipitable water (total column water vapor), t is time, $< >$ indicate a vertical integration from 1000 to 100 hPa, ∇ is the horizontal gradient operator, q is the specific humidity, $\mathbf{V}$ is the horizontal vector wind, E is evaporation and P is precipitation. In the equation (1), there is an assumption involved, that is, the condensates immediately fall out to the surface as precipitation after they form. Although w and q differ between the present-day state and the future climate state, they are assumed to be in an equilibrium state within both the periods. Thus, for each period the tendency term ($\partial w/\partial t$) vanishes. The diagnostic equation of GMP change is then derived based on the difference of remaining terms between the present-day and global warming periods. The change of the GMP may be attributed to changes in horizontal moisture advection, moisture convergence associated with mass convergence (or vertical motion) and surface evaporation, as shown in the following equation:

$$\Delta\mathrm{GMP} = -\Delta<\mathbf{V}\cdot\nabla q> - \Delta<q\nabla\cdot\mathbf{V}> + \Delta\mathrm{E} \qquad (2)$$

The operator Δ ( ) represents the difference between the global warming and present-day simulations (future minus present-day).

[11] The diagnosis result shows that the increase of both the moisture convergence and surface evaporation contribute to the positive GMP trend, whereas moisture advection contributes insignificantly to the GMP increase (Figure 2, top). Whereas the moisture convergence plays a more important role in the ECHAM5, the surface evaporation seems dominant in the GMP increase in the MRI AGCM

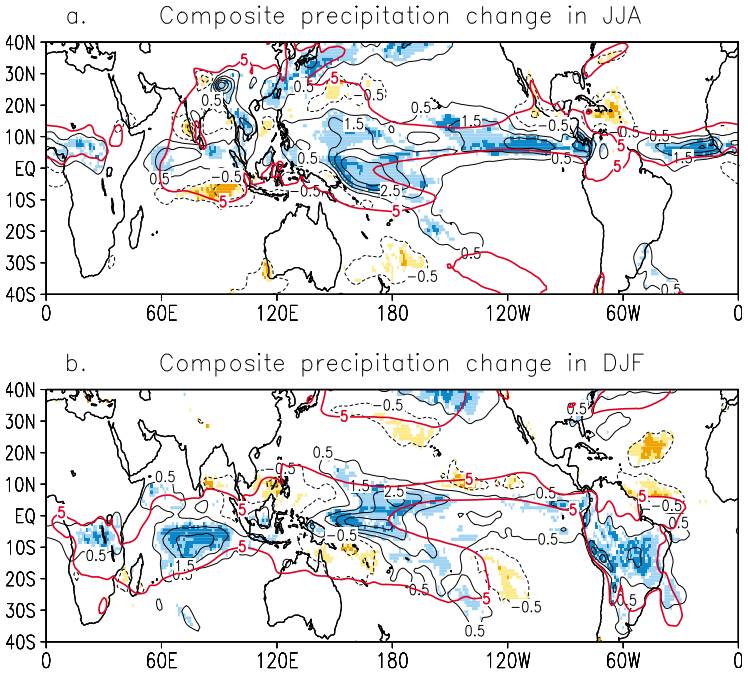

Figure 3. Robust signals of precipitation change. Difference of (a) JJA and (b) DJF mean precipitation fields (contour, unit: mm day^{-1}) between the global warming and present-day simulations. The composite precipitation anomalies from five simulations (T106_mw, T106_sw, T319_sw, MRI_sw.e and GFDL_sw.e) were used. The dark (light) blue shadings indicate that all five (any four) simulations project a consistent increasing trend. The dark (light) yellow shadings indicate that the all five (any four) simulations project a consistent decreasing trend. Only the precipitation change greater than 0.5 mm day^{-1} is shown. Red line shows 5 mm day^{-1} contour of the precipitation climatology composite in the present-day simulations.

and HiRAM simulations. This difference is attributed to model physics and SST warming patterns.

[12] As the changes of atmospheric moisture and circulation affect both the moisture convergence and surface evaporation, it is necessary to reveal their relative contributions. The changes of the moisture convergence and surface evaporation may be decomposed into three terms each, as shown below:

$$-\Delta<q * D> = -<q_{pd} * \Delta D> - <\Delta q * D_{pd}> - <\Delta q * \Delta D> \quad (3)$$

$$\Delta E = \Delta[\alpha|\mathbf{V}|(q_s - q_a)] = \alpha[\Delta|\mathbf{V}| * (q_s - q_a)_{pd} + |\mathbf{V}|_{pd} * \Delta(q_s - q_a) + \Delta|\mathbf{V}| * \Delta(q_s - q_a)] \quad (4)$$

where D denotes the divergence, $\alpha = L\,\rho\,C_E$, L is the latent heat, ρ is the air density at the standard sea-level, C_E is the exchange coefficient, |V| is the surface wind speed, q_s and q_a are the specific humidity at sea surface and at the 10 m respectively, and subscript 'pd' denotes the present-day simulation. The first term in the right-hand side of equations (3) and (4) is associated with the circulation change, which may be regarded as a dynamic contributor. The second term involves the change of water vapor content, thus it reflects the thermodynamic effect on the GMP. The third term is a nonlinear term including the effect of both the moisture and circulation changes. It turns out that the thermodynamic effect due to the increase of atmospheric moisture plays a crucial role in enhancing both the moisture convergence and surface evaporation. The dynamic effect is much weaker and contributes negatively to the GMP increase (Figures 2, middle and 2, bottom). The nonlinear terms are negligible in all the simulations. The results are in general consistent with previous theoretical and modeling studies [*Held and Soden*, 2006; *Chou et al.*, 2009; *Seager et al.*, 2010; *Cherchi et al.*, 2011].

[13] To demonstrate the robust signal of the precipitation change among the five simulations, we define 100% (80%) robustness when the signs of future rainfall projections are same among all five (any four) simulations. Figure 3 highlights areas with consistent JJA and DJF rainfall projections among all five simulations in dark shading (100% robustness) and among any four simulations in light shading (80% robustness) respectively. Here the red contours denote main composite rainfall regions (exceeding 5 mm day^{-1}) in the present-day climate. Note that the projected rainfall increases over most, but not all, of the tropical regions. A consistent increase occurs along the Intertropical Convergence Zone (ITCZ) in northern summer and over the southern Indian Ocean, South America and Southwest Africa in northern winter. Rainfall increases in the central equatorial Pacific all year along, in association with the decrease of the Pacific Walker circulation [*Held and Soden*, 2006; *Li et al.*, 2010]. A marked decrease of rainfall appears south of the equator over the Indian Ocean and Caribbean Sea in boreal summer and over South China Sea, northeast of Australia and Northwestern Atlantic in boreal winter. The complicated rainfall projection result suggests that the rich does not always get richer. Our analysis by comparing the simulation results between the T106_mw and T106_sw suggests that although the enhanced water vapor content is primarily

responsible for overall increase of global precipitation, the change of circulation associated with anomalous SST warming patterns determines regional-scale rainfall changes. Other effects, such as the upped-ante mechanisms associated with dry advection, the deepening of convection related to atmospheric stability and the SST pattern induced oceanic feedback, may also contribute to the regional precipitation changes [*Chou et al.*, 2009].

4. Conclusion

[14] The current high-resolution AGCM simulations and most of the CMIP5/CMIP3 CGCMs project an increasing trend of the global monsoon area, precipitation and intensity under a future warmer climate. It implies that the increase of the global monsoon area and the global monsoon precipitation is a robust signal among the models and SST patterns explored; such an increase has occurred during the past three decades [*Hsu et al.*, 2011; *Wang et al.*, 2012] and will continue to be scripted throughout the 21st century. This is similar to the findings of *Cherchi et al.* [2011] which indicated that the global monsoon rainfall tends to enhance when the CO_2 concentration grows. Through the diagnosis of the moisture budget, one may reveal how much of the GMA change due to global warming is attributed to the change of atmospheric circulation and moisture. Our results indicate that the precipitation change under global warming is primarily due to the warmer temperature induced anomalous hydrological cycle. The increases of horizontal moisture convergence and surface evaporation play an important role in the GMP enhancement, whereas the moisture advection effect is weak. As the increase of atmospheric water vapor contributes positively to the moisture convergence, this convergence effect is partly offset by the weakening of the monsoon circulation due to the increase of static stability. The enhanced surface evaporation is primarily attributed to the increase of surface water vapor associated with the SST warming.

[15] **Acknowledgments.** Comments from Dr. Chia Chou and an anonymous reviewer are greatly appreciated. This work was supported by NSF grant AGS-1106536, ONR grants N000140810256 and N000141010774, and by the International Pacific Research Center that is sponsored by the Japan Agency for Marine-Earth Science and Technology (JAMSTEC), NASA and NOAA. This is SOEST contribution number 8568 and IPRC contribution number 860.

[16] The Editor thanks the two anonymous reviewers for their assistance in evaluating this paper.

References

Bengtsson, L., M. Botzet, and M. Esch (1996), Will greenhouse gas-induced warming over the next 50 years lead to higher frequency and greater intensity of hurricanes?, *Tellus, Ser. A*, *48*, 57–73, doi:10.1034/j.1600-0870.1996.00004.x.

Bretherton, C. S., J. R. McCaa, and H. Grenier (2004), A new parameterization for shallow cumulus convection and its application to marine subtropical cloud-topped boundary layers. Part I: Description and 1D results, *Mon. Weather Rev.*, *132*, 864–882, doi:10.1175/1520-0493(2004)132<0864:ANPFSC>2.0.CO;2.

Cherchi, A., A. Alessandri, S. Masina, and A. Navarra (2011), Effects of increased CO_2 levels on monsoons, *Clim. Dyn.*, *37*, 83–101, doi:10.1007/s00382-010-0801-7.

Chou, C., and C.-W. Lan (2012), Changes in the annual range of precipitation under global warming, *J. Clim.*, *25*, 222–235, doi:10.1175/JCLI-D-11-00097.1.

Chou, C., J. D. Neelin, C.-A. Chen, and J.-Y. Tu (2009), Evaluating the "rich-get-richer" mechanism in tropical precipitation change under global warming, *J. Clim.*, *22*, 1982–2005, doi:10.1175/2008JCLI2471.1.

Held, I. M., and B. J. Soden (2006), Robust responses of the hydrological cycle to global warming, *J. Clim.*, *19*, 5686–5699, doi:10.1175/JCLI3990.1.

Hsu, P.-C., T. Li, and B. Wang (2011), Trends in global monsoon area and precipitation over the past 30 years, *Geophys. Res. Lett.*, *38*, L08701, doi:10.1029/2011GL046893.

Jungclaus, H., et al. (2006), Ocean circulation and tropical variability in the coupled model ECHAM5/MPO-OM, *J. Clim.*, *19*, 3952–3972, doi:10.1175/JCLI3827.1.

Kim, H.-J., B. Wang, and Q. Ding (2008), The global monsoon variability simulated by CMIP3 coupled climate models, *J. Clim.*, *21*, 5271–5294, doi:10.1175/2008JCLI2041.1.

Li, T., M. Kwon, M. Zhao, J.-S. Kug, J.-J. Luo, and W. Yu (2010), Global warming shifts Pacific tropical cyclone location, *Geophys. Res. Lett.*, *37*, L21804, doi:10.1029/2010GL045124.

Liu, J., B. Wang, Q. Ding, X. Kuang, W. Soon, and E. Zorita (2009), Centennial variations of the global monsoon precipitation in the last millennium: Results from ECHO-G model, *J. Clim.*, *22*, 2356–2371, doi:10.1175/2008JCLI2353.1.

Meehl, G. A., C. Covey, T. Delworth, M. Latif, B. McAvaney, J. F. B. Mitchell, R. J. Stouffer, and K. E. Taylor (2007), The WCRP CMIP3 multimodel dataset: A new era in climate change research, *Bull. Am. Meteorol. Soc.*, *88*, 1383–1394, doi:10.1175/BAMS-88-9-1383.

Mizuta, R., et al. (2006), 20-km-mesh global climate simulations using JMA-GSM model–mean climate states, *J. Meteorol. Soc. Jpn.*, *84*, 165–185, doi:10.2151/jmsj.84.165.

Neelin, J. D., M. Münnich, H. Su, J. E. Meyerson, and C. E. Holloway (2006), Tropical drying trends in global warming models and observations, *Proc. Natl. Acad. Sci. U. S. A.*, *103*, 6110–6115, doi:10.1073/pnas.0601798103.

Nordeng, T. E. (1994), Extended versions of the convective parameterization scheme at ECMWF and their impact on the mean and transient activity of the model in the tropics, *Tech. Rep. 206*, 41 pp., Eur. Cent. for Medium-Range Weather Forecasts, Reading, U. K.

Randall, D., and D. Pan (1993), Implementation of the Arakawa–Schubert cumulus parameterization with a prognostic closure, in *The Representation of Cumulus Convection in Numerical Models*, *Meteorol. Monogr.*, vol. 46, pp. 137–144, Am. Meteorol. Soc., Boston, Mass.

Roeckner, E., et al. (2003), The atmospheric general circulation model ECHAM5, Part I: Model description, *Rep. 349*, 127 pp., Max Planck Inst. for Meteorol., Hamburg, Germany.

Seager, R., N. Naik, and G. A. Vecchi (2010), Thermodynamic and dynamic mechanisms for large-scale changes in the hydrological cycle in response to global warming, *J. Clim.*, *23*, 4651–4668, doi:10.1175/2010JCLI3655.1.

Tiedtke, M. (1989), A comprehensive mass flux scheme for cumulus parameterization in large-scale models, *Mon. Weather Rev.*, *117*, 1779–1800, doi:10.1175/1520-0493(1989)117<1779:ACMFSF>2.0.CO;2.

Trenberth, K. E., D. P. Stepaniak, and J. M. Caron (2000), The global monsoon as seen through the divergent atmospheric circulation, *J. Clim.*, *13*, 3969–3993, doi:10.1175/1520-0442(2000)013<3969:TGMAST>2.0.CO;2.

Wang, B., and Q. Ding (2006), Changes in global monsoon precipitation over the past 56 years, *Geophys. Res. Lett.*, *33*, L06711, doi:10.1029/2005GL025347.

Wang, B., J. Liu, H.-J. Kim, P. J. Webster, and S.-Y. Yim (2012), Recent change of the global monsoon precipitation (1979–2008), *Clim. Dyn.*, doi:10.1007/s00382-011-1266-z, in press.

Webster, P. J. (1987), The elementary monsoon, in *Monsoons*, edited by J. S. Fein and P. L. Stephens, pp. 3–32, Wiley-Intersci., New York.

Xie, S.-P., C. Deser, G. A. Vecchi, J. Ma, H. Teng, and A. T. Wittenberg (2010), Global warming pattern formation: Sea surface temperature and rainfall, *J. Clim.*, *23*, 966–986, doi:10.1175/2009JCLI3329.1.

Zhao, M., I. M. Held, S.-J. Lin, and G. A. Vecchi (2009), Simulations of global hurricane climatology, interannual variability, and response to global warming using a 50 km resolution GCM, *J. Clim.*, *22*, 6653–6678, doi:10.1175/2009JCLI3049.1.

P. Hsu and T. Li, International Pacific Research Center, University of Hawaii at Manoa, 1680 East-West Rd., Honolulu, HI 96822, USA. (pangchi@hawaii.edu; timli@hawaii.edu)

A. Kitoh and H. Murakami, Climate Research Department, Meteorological Research Institute, 1-1 Nagamine, Tsukuba, Ibaraki 305-0052, Japan. (kitoh@mri-jma.go.jp; himuraka@mri-jma.go.jp)

J.-J. Luo, Centre for Australian Weather and Climate Research, 700 Collins St., Melbourne, Vic 3008, Australia. (j.luo@bom.gov.au)

M. Zhao, Geophysical Fluid Dynamics Laboratory, NOAA, PO Box 308, U.S. Rte. 1, Princeton, NJ 08542, USA. (ming.zhao@noaa.gov)